
# CTRQ 2024

The Seventeenth International Conference on Communication Theory, Reliability, and Quality of Service

ISBN: 978-1-68558-172-5

May 26 - 30, 2024

Barcelona, Spain

**CTRQ 2024 Editors**

Pascal Lorenz, University of Haute-Alsace, France

# CTRQ 2024

# Forward

The Seventeenth International Conference on Communication Theory, Reliability, and Quality of Service (CTRQ 2024), held between May 26-30, 2024 in Barcelona, Spain, continued a series of events focusing on the achievements in communication theory with respect to reliability and quality of service.

The processing and transmission speed and increasing memory capacity might be a satisfactory solution on the resources needed to deliver ubiquitous services, under guaranteed reliability and satisfying the desired quality of service. Successful deployment of communication mechanisms guarantees decent network stability and offers reasonable control on the quality of service expected by the end users. Recent advances on communication speed, hybrid wired/wireless, network resiliency, delay-tolerant networks and protocols, signal processing and so forth asked for revisiting some aspects of the fundamentals in communication theory. Mainly network and system reliability and quality of service are those that affect the maintenance procedures, on the one hand, and user satisfaction on service delivery, on the other hand. Reliability assurance and guaranteed quality of services require particular mechanisms that deal with dynamics of system and network changes, as well as with changes in user profiles. The advent of content distribution, IPTV, video-on-demand and other similar services accelerate the demand for reliability and quality of service.

We take here the opportunity to warmly thank all the members of the CTRQ 2024 technical program committee, as well as all the reviewers. The creation of such a high-quality conference program would not have been possible without their involvement. We also kindly thank all the authors who dedicated much of their time and effort to contribute to CTRQ 2024. We truly believe that, thanks to all these efforts, the final conference program consisted of top-quality contributions. We also thank the members of the CTRQ 2024 organizing committee for their help in handling the logistics of this event.

We hope that CTRQ 2024 was a successful international forum for the exchange of ideas and results between academia and industry and for the promotion of progress in the areas of Communication Theory, Reliability, and Quality of Service. We also hope that Barcelona provided a pleasant environment during the conference and everyone saved some time to enjoy the historic charm of the city

**CTRQ 2024 Chairs**

**CTRQ Steering Committee**

Kiran Makhijani, FutureWei, USA
Ali Jalooli, California State University at Dominguez Hills, USA
Costas Vassilakis, University of the Peloponnese – Tripoli, Greece

**CTRQ Publicity Chairs**

Laura Garcia, Universitat Politecnica de Valencia, Spain
Sandra Viciano Tudela, Universitat Politecnica de Valencia, Spain

# CTRQ 2024

# Committee

### CTRQ Steering Committee

Kiran Makhijani, FutureWei, USA
Ali Jalooli, California State University at Dominguez Hills, USA
Costas Vassilakis, University of the Peloponnese – Tripoli, Greece

### CTRQ 2024 Publicity Chairs

Laura Garcia, Universidad Politécnica de Cartagena, Spain
Sandra Viciano Tudela, Universitat Politecnica de Valencia, Spain

### CTRQ 2024 Technical Program Committee

Michael Atighetchi, Raytheon BBN, USA
Jasmina Barakovic Husic, BH Telecom, Joint Stock Company / University of Sarajevo, Bosnia and Herzegovina
Sara Berri, CY Cergy Paris University | ENSEA | CNRS, France
Eugen Borcoci, University Politehnica of Bucharest, Romania
Christos Bouras, University of Patras, Greece
Hao Che, University of Texas at Arlington, USA
Daniele Codetta-Raiteri, Università del Piemonte Orientale, Italy
Phuc Do, Lorraine University, France
Szalai Elke, Fachhochschule Burgenland, Austria
Rita Girao-Silva, University of Coimbra & INESC-Coimbra, Portugal
Apostolos Gkamas, University of Ioannina, Greece
Lucian Grigorie, Military Technical Academy "Ferdinand I", Bucharest, Romania
Lav Gupta, University of Missouri - St. Louis, USA
Ilias Iliadis, IBM Research, Zurich, Switzerland
Benoit Iung, Lorraine University, France
Faouzi Jaidi, University of Carthage, Higher School of Communications of Tunis & National School of Engineers of Carthage, Tunisia
Ali Jalooli, California State University Dominguez Hills, USA
Jinlei Jiang, Tsinghua University, China
Laxima Niure Kandel, Embry-Riddle Aeronautical University, USA
Sokratis K. Katsikas, Norwegian University of Science and Technology, Norway
Sondes Ksibi, University of Carthage | Higher School of Communications of Tunis, Tunisia
Ajey Kumar, Symbiosis Centre for Information Technology, India
Mikel Larrea, University of the Basque Country UPV/EHU, Spain
Tong Li, Renmin University of China, China
Dengzhi Liu, Jiangsu Ocean University, China
Sassi Maaloul, Higher Communications School of Tunis (SUP'COM), Tunisia
Kiran Makhijani, FutureWei, USA
Zoubir Mammeri, IRIT - Paul Sabatier University, Toulouse, France
Glenford Mapp, Middlesex University, UK

**Copyright Information**

For your reference, this is the text governing the copyright release for material published by IARIA.

The copyright release is a transfer of publication rights, which allows IARIA and its partners to drive the dissemination of the published material. This allows IARIA to give articles increased visibility via distribution, inclusion in libraries, and arrangements for submission to indexes.

I, the undersigned, declare that the article is original, and that I represent the authors of this article in the copyright release matters. If this work has been done as work-for-hire, I have obtained all necessary clearances to execute a copyright release. I hereby irrevocably transfer exclusive copyright for this material to IARIA. I give IARIA permission or reproduce the work in any media format such as, but not limited to, print, digital, or electronic. I give IARIA permission to distribute the materials without restriction to any institutions or individuals. I give IARIA permission to submit the work for inclusion in article repositories as IARIA sees fit.

I, the undersigned, declare that to the best of my knowledge, the article is does not contain libelous or otherwise unlawful contents or invading the right of privacy or infringing on a proprietary right.

Following the copyright release, any circulated version of the article must bear the copyright notice and any header and footer information that IARIA applies to the published article.

IARIA grants royalty-free permission to the authors to disseminate the work, under the above provisions, for any academic, commercial, or industrial use. IARIA grants royalty-free permission to any individuals or institutions to make the article available electronically, online, or in print.

IARIA acknowledges that rights to any algorithm, process, procedure, apparatus, or articles of manufacture remain with the authors and their employers.

I, the undersigned, understand that IARIA will not be liable, in contract, tort (including, without limitation, negligence), pre-contract or other representations (other than fraudulent misrepresentations) or otherwise in connection with the publication of my work.

Exception to the above is made for work-for-hire performed while employed by the government. In that case, copyright to the material remains with the said government. The rightful owners (authors and government entity) grant unlimited and unrestricted permission to IARIA, IARIA's contractors, and IARIA's partners to further distribute the work.

**Table of Contents**

# Relations Between Entity Sizes and Error-Correction Coding Codewords and Data Loss

Ilias Iliadis
IBM Research Europe – Zurich
8803 Rüschlikon, Switzerland
email: ili@zurich.ibm.com

***Abstract*—Erasure-coding redundancy schemes are employed in storage systems to cope with device and component failures. Data durability is assessed by the Mean Time to Data Loss** (MTTDL) **and the Expected Annual Fraction of Entity Loss** (EAFEL) **reliability metrics. In particular, the** EAFEL **metric assesses losses at an entity, say file, object, or block level. This metric is affected by the number of codewords that entities span. The distribution of this number is obtained analytically as a function of the size of the entities and the frequency of their occurrence. The deterministic and the random entity placement cases are investigated. It is established that for certain deterministic placements of variable-size entities, the distribution of the number of codewords that entities span also depends on the actual entity placement. To evaluate the durability of storage systems in the case of variable-size entities, we introduce the Expected Annual Fraction of Effective Data Loss** (EAFEDL) **reliability metric, which assesses the fraction of stored user data that is lost by the system annually at the entity level. The** EAFEL **and** EAFEDL **metrics are assessed analytically for erasure-coding redundancy schemes and for the clustered, declustered, and symmetric data placement schemes. It is demonstrated that an increased variability of entity sizes results in improved** EAFEL**, but degraded** EAFEDL**. It is established that both reliability metrics are adversely affected by the size of the erasure-coding symbols.**

***Keywords–Reliability analysis; MTTDL; EAFDL; EAFEL; MDS codes; Unrecoverable or latent sector errors; Deferred recovery or repair; stochastic modeling.***

## I. INTRODUCTION

The durability of data storage systems and cloud offerings is affected by device and component failures. Desired reliability levels are ensured by employing erasure-coding redundancy schemes for recovering lost data [1-4].

The frequency of data loss events is assessed by the Mean Time to Data Loss (MTTDL) metric that has been widely used to assess the reliability of storage systems [3][4]. Also, the amount of data loss is obtained by the Expected Annual Fraction of Data Loss (EAFDL) metric that was introduced in [5]. This metric was recently complemented by the Expected Annual Fraction of Entity Loss (EAFEL) metric [6]. The EAFEL metric assesses data losses at an *entity*, say file, object, or block level, whereas the EAFDL metric assesses data losses at a lower data processing unit level.

The smallest accessed unit of a storage device is a *sector* in Hard-Disk Drives (HDDs), a *page* in flash-based Solid-State Drives (SSDs), and a *data set* in Linear Tape-Open (LTO is the trademark of HP, IBM, and Quantum in the Unites States and other countries) tape systems [7]. A sector has a typical size of 512 bytes or 4 KB, a page has a size that ranges from 4 KB to 16 KB, and a data set currently has a size of 5 MB or more. Erasure-coding redundancy schemes are implemented by treating the units that contain user data as symbols and complementing them with parity symbols (units) to form codewords. In the case of HDDs and SSDs, one or more units are allocated to an entity and the last unit may be partially filled. Depending on the file system employed, the remaining space of a partially-filled unit may or may not be used to store the contents of another entity. Therefore, user data may or may not be stored in an aligned fashion with units (symbols), which in turn implies that entities may or may not be aligned with codewords. The case where entities are aligned with codewords was considered by the reliability model presented in [6]. By contrast, in the case of tape, user data is written sequentially such that a unit may contain data of multiple entities. Therefore, user data and entities are not aligned with symbols and codewords, respectively. Moreover, the reliability model presented in [6] assumed that entities have a fixed size, whereas in practice they have variable sizes. It turns out that the MTTDL metric does not depend on the placement and size of the entities, but the EAFEL metric does. More specifically, EAFEL depends on the number of codewords that stored entities span. Furthermore, the EAFEL metric reflects the fraction of lost user data only when entities have a fixed size. To evaluate system durability in the case of variable-size entities, in this article we introduce the Expected Annual Fraction of Effective Data Loss (EAFEDL) reliability metric, that is, the fraction of stored user data that is expected to be lost by the system annually at the entity level.

The key contributions of this article are the following. The reliability model presented in [6] for the assessment of the EAFEL metric is enhanced in two ways. First, entities are considered to be stored such that they are not aligned with codeword boundaries. Second, the size of entities is considered to be variable. The objective of this article is to assess system reliability by deriving the distribution of the number of codewords that entities span. We address the following question. Does this distribution only depend on the statistics of the entities stored, that is, on their size and frequency of occurrence, or does it also depend on their placement? In the present work, we shed light on this issue by investigating the cases of deterministic and of random entity placement. The distribution of the number of codewords that entities span is obtained analytically as a function of the size of the entities and the frequency of their occurrence. We also establish that for certain deterministic placements of variable-size entities, this distribution also depends on the actual entity placement.

The general non-Markovian methodology that was applied in prior work to assess the EAFDL and EAFEL metrics for erasure-coding redundancy schemes and for the clustered, declustered, and symmetric data placement schemes, is ex-

TABLE I. NOTATION OF SYSTEM PARAMETERS

| Parameter | Definition |
|---|---|
| $n$ | number of storage devices |
| $c$ | amount of data stored on each device |
| $l$ | number of user-data symbols per codeword ($l \geq 1$) |
| $m$ | total number of symbols per codeword ($m > l$) |
| $(m, l)$ | MDS-code structure |
| $e_s$ | entity size |
| $s$ | symbol size |
| $s_{\text{eff}}$ | storage efficiency of redundancy scheme ($s_{\text{eff}} = l/m$) |
| $U$ | amount of user data stored in the system ($U = s_{\text{eff}}\, n\, c$) |
| $\tilde{r}$ | MDS-code distance: minimum number of codeword symbols lost that lead to permanent data loss ($\tilde{r} = m - l + 1$ and $2 \leq \tilde{r} \leq m$) |
| $C$ | number of symbols stored in a device ($C = c/s$) |
| $s_s$ | shard size ($s_s = e_s/l$) |
| $J$ | shard size measured in symbol-size units ($J = s_s/s = e_s/(l\, s)$) |
| $Y$ | number of lost entities during rebuild |
| $\breve{Q}$ | amount of lost user data during rebuild |

tended to derive analytically the EAFEL and the new EAFEDL reliability metrics for the case of variable-size entities. Subsequently, we demonstrate the effect of erasure-coding capability as well as of entity and symbol sizes on system reliability for the entire range of bit error rates.

The remainder of the article is organized as follows. Section II describes the storage system model and the corresponding parameters considered. In Section III, the distribution of the number of codewords that entities span is derived analytically as a function of the entity size distribution when entities are not aligned with symbols and when entity sizes are either fixed or variable. In Section IV, the EAFEL and EAFEDL metrics are derived analytically for the case of random placement of variable-size entities. Section V presents numerical results demonstrating the effect of the erasure-coding capability and of the entity sizes on system reliability, as well as the adverse effect of an increased symbol size. Finally, we conclude in Section VI.

## II. STORAGE SYSTEM MODEL

The reliability of erasure-coded storage systems was assessed in [6] based on a model that considers codeword rebuilds for reconstructing lost symbols and assess system reliability when entities (files, objects, blocks) are lost. Maximum Distance Separable (MDS) erasure codes $(m, l)$ that map $l$ user-data symbols to codewords of $m$ symbols are employed. They have the property that any subset containing $l$ of the $m$ codeword symbols can be used to reconstruct (recover) a codeword. The MTTDL and EAFEL reliability metrics were derived analytically for systems that employ a lazy rebuild scheme.

The corresponding storage efficiency $s_{\text{eff}}$ and amount $U$ of user data stored in the system is

$$s_{\text{eff}} = l/m \quad \text{and} \quad U = s_{\text{eff}}\, n\, c \;=\; l\, n\, c/m\;, \qquad (1)$$

where $n$ is the number of storage devices in the system and $c$ is the amount of data stored on each device. Also, the number $C$ of symbols stored in a device is

$$C = c/s\;. \qquad (2)$$

Our notation is summarized in Table I. The parameters are divided according to whether they are independent or derived and are listed in the upper and lower part of the table, respectively.

To minimize the risk of permanent data loss, the $m$ symbols of each of codeword are spread and stored in $m$ devices. This way, the system can tolerate any $\tilde{r} - 1$ device failures, but $\tilde{r}$ device failures may lead to data loss, with

$$\tilde{r} = m - l + 1\;, \quad 1 \leq l < m \quad \text{and} \quad 2 \leq \tilde{r} \leq m\;. \qquad (3)$$

Two different ways (A and B) for storing user data on devices were shown in Figure 1 of [6]. According to way A, user data contained in entities is divided into chunks with the contents of a chunk stored on different devices, whereas according to way B, user data contained in entities is divided into *shards* with the contents of a shard stored on the same device. More specifically, according to way B, user data contained in entities is divided into $l$ shards with each one being stored on a different device, as shown in Figure 1(a). Entities were assumed to have a fixed size $e_s$ with the corresponding shard size $s_s$ then obtained by $s_s = e_s/l$.

The storage space of devices is partitioned into units (symbols) of a fixed size $s$ and complemented with parity symbols to form codewords. Each shard was assumed to be stored in an integer number of $J$ symbols that is determined by

$$J = \frac{s_s}{s} = \frac{e_s}{l\, s}\;. \qquad (4)$$

Consequently, the contents of each entity, such as Entity-1 and Entity-2, are stored in $J\, l$ user-data symbols with these symbols being stored in an integer number of $J$ codewords. These codewords also contain $J\,(m - l)$ parity symbols for a total number of $J\, m$ symbols per entity, as shown in Figure 1(a). Note that $S_{j,i}$ denotes the $i$th symbol of the $j$th codeword. Thus, $S_{1,2}$, which is the second symbol of codeword C-1, is the first symbol of the second shard. Successive symbols of a shard are stored on the same device. To minimize the risk of permanent data loss, the $m$ symbols of each of the $J$ codewords are spread and stored successively in a set of $m$ devices.

The model in [6] considered shards that have a fixed size of $J$ symbols and are stored aligned with the symbol boundaries, which are indicated by the horizontal black lines in Figure 1(a). However, in practice user entities, and in turn shards, do not have a fixed size and, in the case of tape, are not necessarily aligned with symbols, because, as discussed in Section I, entity data is stored in a way that is agnostic to symbol boundaries. This is demonstrated in Figure 1(b) that shows two entities of two different sizes, Entity-3 and Entity-4, and the way they are stored on $l$ devices of the system. For instance, Shard 1 of Entity-3 spans $J$ symbols, i.e., the blue symbols $S_{1,1}$, $S_{2,1}$, $\cdots$ , $S_{J,1}$, with its data partially occupying the first and last symbol, $S_{1,1}$ and $S_{J,1}$, respectively. Subsequently, Shard 1 of Entity-4 spans three symbols, namely, the blue symbol $S_{J,1}$ and the two red symbols $S_{1,1}$ and $S_{2,1}$, with its data partially occupying the first and the last symbol, that is, the blue $S_{J,1}$ and the red $S_{2,1}$ symbol. Thus, symbol $S_{J,1}$ contains data from both these entities. More generally, depending on the entity and symbol sizes, a symbol may contain data from multiple entities. Clearly, shard and entity sizes do not necessarily correspond to an integer number of symbols, which implies that the size $J$ of a shard, expressed in number of symbols by (4), is in general a real number, which is less than 1 when the shard size is less than the symbol size. Codewords are formed by combining symbols containing user-data to generate and store parity symbols, as shown in Figure 1(b), regardless of the entities involved.

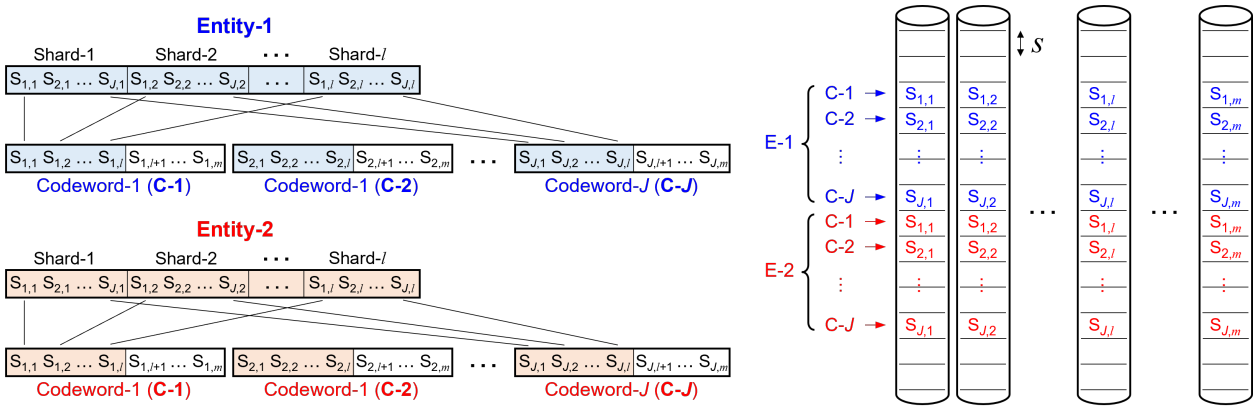


(a) Symbol-aligned shards of integer size

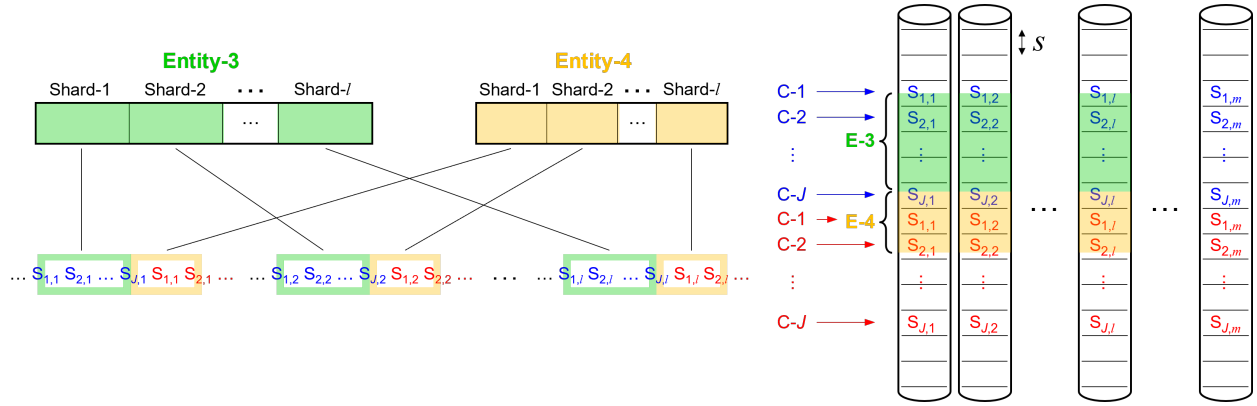


(b) Non-symbol-aligned shards of arbitrary size

Figure 1. Data placement of entities and formation of codewords.

As pointed out in [6], the MTTDL metric does not depend on the entity size. This is due to the fact that the degree to which permanent data losses occur depends on the capability of the erasure-coding redundancy scheme employed and the resulting codeword formation, which in turn is agnostic to the entity placement and size characteristics. Note that an entity is lost if any of the codewords that it spans is permanently lost. Consequently, the EAFEL and EAFEDL metrics, which consider data loss at the entity level, depend on the number of codewords that entities span. The corresponding derivation is performed in Section III.

The reliability of storage systems degrades by the presence of unrecoverable or latent errors. According to the specifications of enterprise quality HDDs, the unrecoverable bit-error probability $P_{\rm b}$ is equal to $10^{-15}$. In practice, however, $P_{\rm b}$ can be orders of magnitude higher, reaching $P_{\rm b} \approx 10^{-12}$ [4]. On the other hand, according to Figure 13 in [8], tapes are more reliable than HDDs with a Bit Error Rate (BER) in the range of $10^{-22}$ to $10^{-19}$. Assuming that bit errors occur independently over successive bits, the unrecoverable symbol error probability $P_s$ is determined by

$$P_s = 1 - (1 - P_{\rm b})^s \,, \tag{5}$$

with the symbol size $s$ expressed in bits. Moreover, latent errors are found to exhibit spatial locality and they occur in bursts of multiple contiguous symbol errors. The degree to which symbol errors are correlated is captured by the factor $f_{\rm cor}$ whose value is typically close to 1 [4].

## III. Codewords Spanned by Entities

Here, we obtain the distribution of the number of codewords, $K$, that entities span, which also represents the number of symbols that shards span. We proceed by considering the cases of fixed- and variable-size entities (shards).

### A. Fixed-Size Entities

Let us consider fixed-size entities, which in turn result in fixed-size shards, such that $J$ is fixed. Owing to periodicity, it suffices to study the process within a window of $S = J \times 10^k$ symbols, where $k$ represents the number of decimal digits of $J$. This window corresponds in a symbol interval $[\epsilon, S + \epsilon]$ with $0 < \epsilon < 1$. This interval contains $S$ symbol boundaries and stores $10^k$ shards. For example, for $J = 4.287$, we have $k = 3$, and it suffices to consider the process in a window of $S = 4.287 \times 10^3 = 4,287$ symbols that store 1000 shards.

Let us now consider the example shown in Figure 2 whereby the shard size is 2.3. In this case, it holds that $k = 1$ and therefore it suffices to consider the process within a window of $S = 2.3 \times 10^1 = 23$ symbols that store 10 shards depicted between the black circles with the symbol boundaries indicated by the black vertical lines and with the first shard aligned with the first symbol. However, given that in practice shards are not aligned with symbols, their actual placement is indicated between the red circles, with the first shard starting at position $\epsilon$, as indicated by the green circle.

Owing to periodicity, it suffices to study the process in the symbol interval $[\epsilon, 23 + \epsilon]$. The red integers indicate the

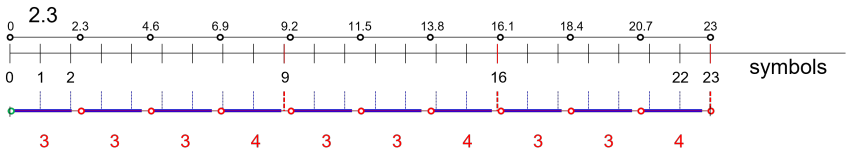


Figure 2. Number of symbols that shards span. Fixed-size shards of size 2.3 symbols.

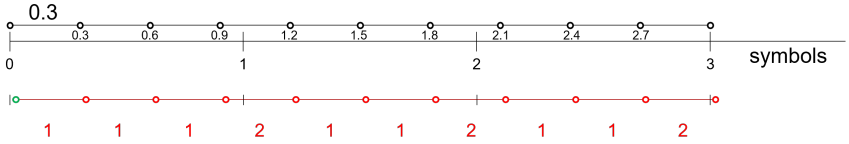


Figure 3. Number of symbols that shards span. Fixed-size shards of size 0.3 symbols.

number of symbols spanned by the successive shards. We note that 7 shards span 3 symbol and the remaining 3 shards span 4 symbols. Therefore, the probability density function (pdf) $\{p_j\}$ of the number of symbols $K$ that an arbitrary shard spans is

$$P(K=i)=p_i=\begin{cases}0.7\,, & \text{for } \ i=3\\ 0.3\,, & \text{for } \ i=4\,.\end{cases} \tag{6}$$

Returning to the general case, we note that each shard can be decomposed into two components. The size of the first components, as indicated by the horizontal blue lines shown in Figure 2, corresponds to the number of symbols determined by the integer part of the shard size $J$, which is $\lfloor J \rfloor$ symbols. In the example considered, the integer part is 2. The size of the second components, as indicated by the horizontal red lines shown in Figure 2, corresponds to the fractional part, which is $J-\lfloor J \rfloor$ symbols. In the example considered, the fractional part is 0.3. Clearly, to each of the first (blue) components correspond $\lfloor J \rfloor$ symbol boundaries, which implies that each shard spans at least $\lfloor J \rfloor + 1$ symbols. In the example considered, to each of the first (blue) components correspond 2 symbol boundaries, as indicated by the blue vertical dotted lines, and, consequently, each shard spans at least 3 symbols.

As there are $10^k$ first components, one for each shard, the number of the corresponding symbol boundaries is $\lfloor J \rfloor \times 10^k$, which, in the example considered, is $2 \times 10^1 = 20$, as indicated by the blue vertical dotted lines. Consequently, there are $S - \lfloor J \rfloor \times 10^k = (J - \lfloor J \rfloor) \times 10^k$ additional symbol boundaries that correspond to $(J - \lfloor J \rfloor) \times 10^k$ out of the $10^k$ second components. In the example considered, there are $23 - 20 = 3$ additional symbol boundaries, as indicated by the red vertical dotted lines at positions 9, 16, and 23, that correspond to 3 out of the 10 red components. Consequently, these 3 components are associated with 3 shards, each of which spans one additional symbol for a total of 4 symbols. In general, each of the corresponding $(J - \lfloor J \rfloor) \times 10^k$ shards spans one additional symbol for a total of $\lfloor J \rfloor + 2$ symbols. Therefore, the percent of shards that span $\lfloor J \rfloor + 2$ symbols is $(J - \lfloor J \rfloor) \times 10^k / 10^k$ which is equal to $J - \lfloor J \rfloor$, that is, the fractional part of $J$ denoted by $fr(J)$. Consequently, for any $\epsilon$ $(0 < \epsilon < 1)$, it holds that

$$P(K=i)=p_i=\begin{cases}1-fr(J)\,, & \text{for } \ i=\lfloor J \rfloor + 1\\ fr(J)\,, & \text{for } \ i=\lfloor J \rfloor + 2\\ 0\,, & \text{otherwise}\,,\end{cases} \tag{7}$$

where $fr(x)$ denotes the fractional part of the real number $x$,

$$fr(x) \triangleq x - \lfloor x \rfloor\,, \quad \forall\, x \in \mathcal{R}\,. \tag{8}$$

Let us also consider the case where $J < 1$ and the example shown in Figure 3 whereby the shard size is 0.3. Let us consider the first 10 shards indicated between the black circles with the first shard aligned with the first symbol. However, given that in practice shards are not aligned with symbols, their actual placement is indicated between the red circles, with the first shard starting at position $\epsilon$, as indicated by the green circle. Owing to periodicity, it suffices to study the process in the symbol interval $[\epsilon, 3+\epsilon]$. The red integers indicate the number of symbols spanned by the successive shards. We note that 7 shards span 1 symbol and the remaining 3 shards span 2 symbols. Therefore, the pdf $\{p_j\}$ of the number of codewords (symbols) $K$ that an arbitrary entity (shard) spans is

$$P(K=i)=p_i=\begin{cases}0.7\,, & \text{for } \ i=1\\ 0.3\,, & \text{for } \ i=2\,,\end{cases} \tag{9}$$

which is also the result determined by (7).

Next, we consider the case where the shard size is 2.7 symbols, as shown in Figure 4. Owing to periodicity, it suffices to study the process in the symbol interval $[\epsilon, 27+\epsilon]$. The red integers indicate the number of symbols spanned by the successive shards. We note that 7 shards span 4 symbol and the remaining 3 shards span 3 symbols. According to (7), the pdf $\{p_j\}$ of the number of codewords (symbols) $K$ that an arbitrary entity (shard) spans is

$$P(K=i)=p_i=\begin{cases}0.3\,, & \text{for } \ i=3\\ 0.7\,, & \text{for } \ i=4\,,\end{cases} \tag{10}$$

which is also the result determined by (7).

### B. *Variable-Size Entities*

We proceed to relax the assumption that all entities have the same size, by considering entities of $L$ different sizes, $e_{s,1}, e_{s,2}, \cdots, e_{s,L}$. Without loss of generality, we assume that $e_{s,1} < e_{s,2} < \cdots < e_{s,L}$. Subsequently, let $\{v_j\}$ denote the corresponding pdf of the entity size, that is,

$$v_j \triangleq P(e_s = e_{s,j})\,, \quad \text{for } \ j=1,2,\ldots,L\,, \tag{11}$$

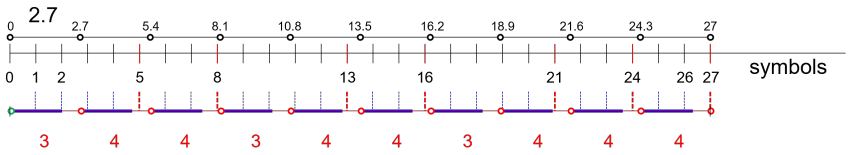


Figure 4. Number of symbols that shards span. Fixed-size shards of size 2.7 symbols.

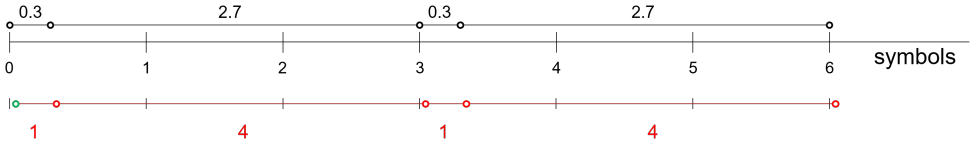


(a) Shard sequence: {0.3, 2.7, 0.3, 2.7, . . . }

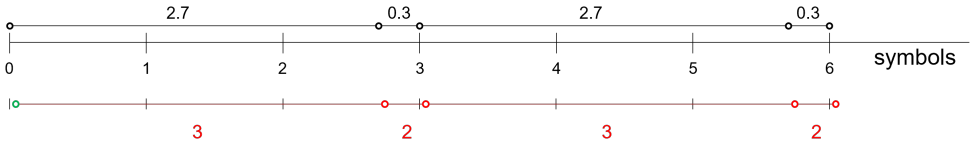


(b) Shard sequence: {2.7, 0.3, 2.7, 0.3, . . . }

Figure 5. Number of symbols spanned by shards. Alternating fixed-size shards of sizes 0.3 and 2.7 symbols, with $v_1 = v_2 = 0.5$.

such that the average entity size $E(e_s)$ is determined by

$$E(e_s) = \sum_{j=1}^{L} e_{s,j}\, v_j \ . \tag{12}$$

From (4), it follows that the shard size $J_j$ corresponding to entity $e_{s,j}$ is determined by

$$J_j = \frac{e_{s,j}}{l\, s} \quad \text{for} \quad j = 1, 2, \ldots, L \ . \tag{13}$$

Consequently, the pdf of the shard size $J$ is determined by

$$P(J = J_j) = v_j \ , \quad \text{for} \quad j = 1, 2, \ldots, L \ , \tag{14}$$

such that the average shard size $E(J)$ is determined by

$$E(J) \ = \sum_{j=1}^{L} J_j\, v_j \ \overset{(12)(13)}{=} \ \frac{E(e_s)}{l\, s} \ . \tag{15}$$

The preceding discussion begs the following questions. Can the probability density function $\{p_j\}$ that was theoretically obtained in (7) for the case of a single fixed shared size be extended for the case of variable-size entities? Does it depend on the sequence according to which the variable-size entities are stored? Next, we address these critical questions. We shed light on these issues by considering the following cases regarding the placement and the way according to which the various shards are stored.

*1) Segregated Shard Placement:* According to this placement, shards of any given size are stored successively. One particular realization is to first store the shards of size $J_1$, followed by the shards of size $J_2$, and so on. For a large number of shards stored, from (7) and (14) we deduce that

$$P(K = i) = p_i = \begin{cases} [1 - fr(J_j)]\, v_j \ , & \text{for} \quad i = \lfloor J_j \rfloor + 1 \\ fr(J_j)\, v_j \ , & \text{for} \quad i = \lfloor J_j \rfloor + 2 \\ 0 \ , & \text{otherwise,} \end{cases}$$
$$\text{for } j = 1, 2, \ldots, L \ . \tag{16}$$

Let us consider the special case of a discrete bimodal distribution for the shard size, that is, $L = 2$, and let us assume that half of the shards have a size of 0.3 symbols and the remaining half of the shards have a size of 2.7 symbols. In this case we have $J_1 = 0.3$, $J_2 = 2.7$, and $v_1 = v_2 = 0.5$. For the particular realization where first the shards of size 0.3 are stored followed by the shards of size 2.7, (16) yields

$$P(K = i) = p_i = \begin{cases} 0.7 \times 0.5 = 0.35 \ , & \text{for} \quad i = 1 \\ 0.3 \times 0.5 = 0.15 \ , & \text{for} \quad i = 2 \\ 0.3 \times 0.5 = 0.15 \ , & \text{for} \quad i = 3 \\ 0.7 \times 0.5 = 0.35 \ , & \text{for} \quad i = 4 \\ 0 \ , & \text{otherwise.} \end{cases} \tag{17}$$

*2) Alternating Shard Placement:* According to this placement, shards of various sizes are stored interleaved by also considering the $v_j$ values. One particular realization in the case where $v_j = 1/L$, for $j = 1, 2, \ldots, L$, is to first store a shard of size $J_1$, followed by a shard of size $J_2$, and so on. The first cycle is completed by storing a shard of size $J_L$ and is followed by a second cycle that begins by storing a shard of size $J_1$.

We proceed by investigating the special case considered in Section III-B1 for the discrete bimodal distribution of the shard size, with the sizes of 0.3 and 2.7 symbols. The alternating placement of the shards corresponding to these two sizes lead to two possible sequence realizations, as shown in Figure 5.

The realization for the alternating sequence $\{0.3, 2.7, 0.3, 2.7, \ldots\}$ is depicted in Figure 5(a). Owing to periodicity, it suffices to study the process in the symbol interval $[\epsilon, 3+\epsilon]$. The red integers indicate the number of symbols spaned by the successive shards. We note that half of the shards span 1 symbol and the remaining half of the shards span 4 symbols. Consequently, the pdf $\{p_j\}$ of the number of symbols $K$ that

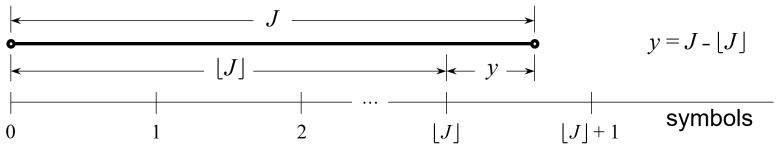


(a) Shard of size $J$ with $y$ being the fractional part of $J$

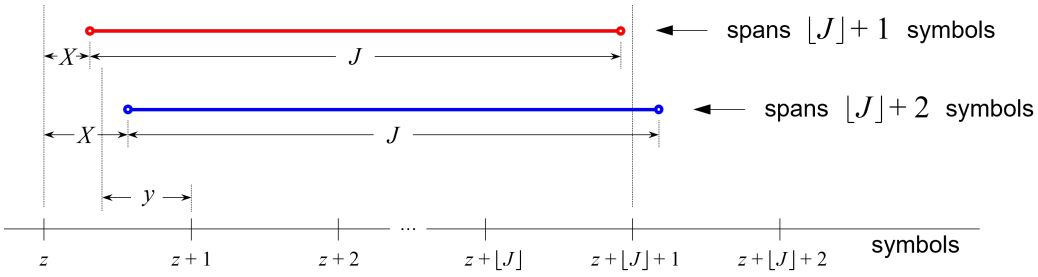


(b) Random shard placement

Figure 6. Number of symbols that a randomly placed shard of size $J$ spans.

an arbitrary shard spans is

$$P(K=i)=p_i=\begin{cases}0.5\,, & \text{for } i=1\\ 0.5\,, & \text{for } i=4\,.\end{cases} \tag{18}$$

On the other hand, the realization for the alternating sequence $\{2.7, 0.3, 2.7, 0.3, \ldots\}$ is depicted in Figure 5(b). In this case, half of the shards span 3 symbols and the remaining half of the shards span 2 symbols. Consequently, the pdf $\{p_j\}$ of the number of symbols $K$ that an arbitrary shard spans is

$$P(K=i)=p_i=\begin{cases}0.5\,, & \text{for } i=2\\ 0.5\,, & \text{for } i=3\,.\end{cases} \tag{19}$$

We now observe that the pdf determined by (19) is different from that determined by (18). Moreover, both of them, are different from that determined by (17) for the case of a segregated shard placement. Therefore, from the above, we deduce that the pdf $\{p_j\}$ of the number of symbols $K$ that an arbitrary shard spans not only depends on the percentage of the various shard sizes in a sequence, as specified in (14), but also on their actual placement.

*3) Random Shard Placement:* According to this placement, successive shard sizes are assumed to be independent and identically distributed (i.i.d) according to the distribution given in (14). Let us consider a randomly chosen shard. Let also $J$ denote its size, as shown in in Figure 6(a), and $y$ its fractional part, that is, $y = J - \lfloor J \rfloor$. A randomly placed such shard spans either $\lfloor J \rfloor + 1$ or $\lfloor J \rfloor + 2$ symbols, as depicted by the red and the blue shards shown in Figure 6(b), respectively. Let $X$ denote the distance between the starting position of the shard and the left boundary $z$ of the first symbol that the shard spans. Owing to the random placement of the shard, the random variable $X$ is uniformly distributed between 0 and 1. Furthermore, when $X \leq 1 - y$, the shard spans $\lfloor J \rfloor + 1$ symbols where as when $X > 1 - y$, the shard spans $\lfloor J \rfloor + 2$ symbols. Consequently, the probability that the shard spans $\lfloor J \rfloor + 1$ symbols is

$$P(K=\lfloor J\rfloor+1)=\int_0^{1-y} dx = 1-y\,, \tag{20}$$

which implies that the probability that the shard spans $\lfloor J \rfloor + 2$ symbols is

$$P(K=\lfloor J\rfloor+2)=1-P(K=\lfloor J\rfloor+1)\overset{(20)}{=}y\,. \tag{21}$$

Therefore, and given that $y = J - \lfloor J \rfloor = fr(J)$, it holds that

$$P(K=i)=p_i=\begin{cases}1-fr(J)\,, & \text{for } i=\lfloor J\rfloor+1\\ fr(J)\,, & \text{for } i=\lfloor J\rfloor+2\\ 0\,, & \text{otherwise}\,.\end{cases} \tag{22}$$

From (22), and using (8), it follows that the mean number $E(K)$ of symbols that a shard of size $J$ spans is

$$\begin{aligned}E(K)&=(\lfloor J\rfloor+1)P(K=\lfloor J\rfloor+1)+(\lfloor J\rfloor+2)P(K=\lfloor J\rfloor+2)\\ &=(\lfloor J\rfloor+1)\,[1-fr(J)]+(\lfloor J\rfloor+2)\,fr(J)=J+1\,.\end{aligned} \tag{23}$$

From (14), (22), and (23), it follows that the pdf and the average number of symbols $K$ that an arbitrary shard spans are determined by

$$P(K=i)=p_i=\begin{cases}[1-fr(J_j)]\,v_j\,, & \text{for } i=\lfloor J_j\rfloor+1\\ fr(J_j)\,v_j\,, & \text{for } i=\lfloor J_j\rfloor+2\\ 0\,, & \text{otherwise,}\end{cases}$$
$$\text{for } j=1,2,\ldots,L\,, \tag{24}$$

and

$$E(K)=\sum_{j=1}^{L}(J_j+1)\,v_j=E(J)+1\,. \tag{25}$$

*Remark 1:* For two different shard-size values, say $J_m \neq J_n$, for which it holds that $\lfloor J_m \rfloor = \lfloor J_n \rfloor = i$, the corresponding probabilities of the number of symbols $K$ that these shards span are determined additively, that is, $P(K = i) = [1 - fr(J_m)]\,v_m + [1 - fr(J_n)]\,v_m$ and $P(K = i + 1) = fr(J_m)\,v_m + [1 - fr(J_n)]\,v_n$. Similarly, if $\lfloor J_m \rfloor + 1 = \lfloor J_n \rfloor + 2 = i$, then it holds that $P(K = i) = fr(J_m)\,v_m + fr(J_n)\,v_n$.

*Remark 2:* From (16) and (24), it follows that the pdfs of the number of symbols $K$ that an arbitrary shard spans in the segregated and the random shard placement cases are the same.

## IV. Derivation of EAFEL and EAFEDL

The EAFEL and EAFEDL reliability metrics are derived using the general methodology presented in [1-5], which we briefly review here. At any point in time, the system is in one of two modes: non-rebuild or rebuild mode. Note that part of the non-rebuild mode is the normal mode of operation where all devices are operational and all data in the system has the original amount of redundancy. Upon device failures, a rebuild process attempts to restore the lost data, which eventually leads the system either to a Data Loss (DL) or back to the original normal mode by restoring initial redundancy.

The EAFEL metric is obtained by Equation (16) of [6] as follows:

$$\text{EAFEL} \approx \frac{E(Y)}{E(T) \cdot N_E} , \tag{26}$$

that is, as the ratio of the expected number $E(Y)$ of lost entities, normalized to the number $N_E$ of entities in the system, to the expected duration $E(T)$, expressed in years, of a typical interval of normal operation until the rebuild process of failed devices is triggered, which is determined by Equation (14) of [6]. The number $N_E$ of entities in the system is

$$N_E \approx \frac{U}{E(e_s)} \overset{(1)}{=} \frac{n}{m} \cdot \frac{l\,c}{E(e_s)} \overset{(15)}{=} \frac{n}{m} \cdot \frac{c}{E(J)\,s} . \tag{27}$$

Similarly to Equation (9) of [5], the EAFEDL is obtained as the ratio of the expected amount $E(\breve{Q})$ of lost user data at the entity level, normalized to the amount $U$ of user data, to the expected duration of $E(T)$ expressed in years:

$$\text{EAFEDL} \approx \frac{E(\breve{Q})}{E(T) \cdot U} \overset{(1)}{=} \frac{m\,E(\breve{Q})}{n\,l\,c\,E(T)} . \tag{28}$$

### A. Reliability Analysis

The EAFEDL is evaluated in parallel with EAFEL using the theoretical framework presented in [6]. The system is at exposure level $u$ $(0 \le u \le \tilde{r})$ when there are codewords that have lost $u$ symbols owing to device failures, but there are no codewords that have lost more symbols. These codewords are referred to as the *most-exposed* codewords. Transitions to higher exposure levels are caused by device failures, whereas transitions to lower ones are caused by successful rebuilds. We denote by $C_u$ the number of most-exposed codewords upon entering exposure level $u$, $(u \ge 1)$. Upon the first device failure it holds that

$$C_1 = C , \tag{29}$$

where $C$ is determined by (2).

The reliability metrics of interest are derived using the *direct path approximation*, which considers only transitions from lower to higher exposure levels [1-5]. This implies that each exposure level is entered only once. At any exposure level $u$ $(u = d+1, \ldots, \tilde{r}-1)$, data loss may occur during rebuild owing to one or more unrecoverable failures, which is denoted by the transition $u \to$ UF. Moreover, at exposure level $\tilde{r}-1$, data loss occurs owing to a subsequent device failure, which leads to the transition to exposure level $\tilde{r}$. Consequently, the direct paths that lead to data loss are the following:

- $\overrightarrow{UF_u}$ : the direct path of successive transitions $1 \to 2 \to \cdots \to u \to$ UF, for $u = d+1, \ldots, \tilde{r}-1$, and
- $\overrightarrow{\text{DF}}$ : the direct path of successive transitions $1 \to 2 \to \cdots \to \tilde{r}-1 \to \tilde{r}$.

*1) Entity Loss:* We proceed to derive the number of lost entities during rebuild. Let $Y$ be the number of lost entities. Let also $Y_{\text{DF}}$ and $Y_{\text{UF}_u}$ denote the number of lost entities associated with the direct paths $\overrightarrow{\text{DF}}$ and $\overrightarrow{UF_u}$, respectively. Then, it holds that [6, Equations (37), (38), (41)]

$$E(Y) \approx E(Y_{\text{DF}}) + \sum_{u=d+1}^{\tilde{r}-1} E(Y_{\text{UF}_u}) \approx E(Y_{\text{DF}}) + E(Y_{\text{UF}}) , \tag{30}$$

where $Y_{\text{UF}}$ denotes the number of lost entities due to unrecoverable failures with its mean given by

$$E(Y_{\text{UF}}) \approx \sum_{u=1}^{\tilde{r}-1} E(Y_{\text{UF}_u}) . \tag{31}$$

*Proposition 1:* For $u = d+1, \ldots, \tilde{r}-1$, it holds that

$$E(Y_{\text{UF}_u}) \approx \frac{C}{E(J)} \frac{P_u}{u-d} \left( \prod_{j=1}^{u-1} V_j \right) \tilde{q}_u , \tag{32}$$

where $\tilde{q}_u$, which denotes the probability that an arbitrary entity is lost, is determined by

$$\tilde{q}_u = \sum_{j=1}^{L} \tilde{q}_{s,u} \left( \frac{e_{s,j}}{l\,s} \right) v_j , \tag{33}$$

with

$$\tilde{q}_{s,u}(x) \triangleq 1 - [1 - fr(x)]\, q_u^{f_{\text{cor}}(\lfloor x \rfloor + 1)} - fr(x)\, q_u^{f_{\text{cor}}(\lfloor x \rfloor + 2)} , \tag{34}$$

and $q_u$, which denotes the probability that a codeword that has lost $u$ symbols can be restored, is determined by

$$q_u = 1 - \sum_{j=\tilde{r}-u}^{m-u} \binom{m-u}{j} P_s^j (1-P_s)^{m-u-j} . \tag{35}$$

It also holds that

$$E(Y_{\text{DF}}) \approx \frac{C}{E(J)} \frac{P_{\text{DF}}}{\tilde{r}-d} \prod_{j=1}^{\tilde{r}-1} V_j , \tag{36}$$

where $C$ is determined by (2), $P_s$ is determined by (5), $fr(x)$ is determined by (8), $E(J)$ is determined by (15), and $P_u$, $P_{\text{DF}}$, and $V_j$ are determined by Equations (29), (23), and (60) of [6], respectively.

*Proof:* Equation (32) is obtained in Appendix. Equation (36) is obtained from (32) by setting $u = \tilde{r}$ and recognizing that $q_{\tilde{r}} = 0$, $\tilde{q}_{s,\tilde{r}}(x) = 1$, $\forall\, x \in \mathcal{R}$, $\tilde{q}_{\tilde{r}} = 1$, and $P_{\tilde{r}} = P_{\text{DF}}$. ■

*2) Effective Amount of Data Loss:* We proceed to derive the effective amount of lost user data during rebuild. Let $\breve{Q}$ be the amount of user data contained in the $Y$ lost entities, which is permanently lost, too. Let also $\breve{Q}_{\text{DF}}$ and $\breve{Q}_{\text{UF}_u}$ denote the amount of lost user data associated with the direct paths $\overrightarrow{\text{DF}}$ and $\overrightarrow{UF_u}$, respectively.

Similarly to (30), it holds that

$$E(\breve{Q}) \approx E(\breve{Q}_{\text{DF}}) + \sum_{u=d+1}^{\tilde{r}-1} E(\breve{Q}_{\text{UF}_u}) \approx E(\breve{Q}_{\text{DF}}) + E(\breve{Q}_{\text{UF}}) , \tag{37}$$

TABLE II. PARAMETER VALUES

| Parameter | Definition | Values |
|---|---|---|
| $n$ | number of storage devices | 64 |
| $c$ | amount of data stored on each device | 20 TB |
| $s$ | symbol (sector) size | 512 B, 5 MB |
| $\lambda^{-1}$ | mean time to failure of a storage device | 876,000 h |
| $b$ | rebuild bandwidth per device | 100 MB/s |
| $m$ | symbols per codeword | 16 |
| $l$ | user-data symbols per codeword | 13, 14, 15 |
| $d$ | lazy rebuild threshold ($0 \leq d < m - l$) | 0, 1, 2 |
| $U$ | amount of user data stored in the system | 1.04 to 1.2 PB |
| $\mu^{-1}$ | time to read an amount $c$ of data at a rate $b$ from a storage device | 55.5 h |

where $\breve{Q}_{\text{UF}}$ denotes the amount of user data lost due to unrecoverable failures with its mean given by

$$E(\breve{Q}_{\text{UF}}) \approx \sum_{u=1}^{\tilde{r}-1} E(\breve{Q}_{\text{UF}_u}) \ . \tag{38}$$

*Proposition 2:* For $u = d+1, \ldots, \tilde{r}-1$, it holds that

$$E(\breve{Q}_{\text{UF}_u}) \approx \frac{C}{E(J)} \frac{P_u}{u-d} \left( \prod_{j=1}^{u-1} V_j \right) \breve{q}_u \ , \tag{39}$$

where the expected amount $\breve{q}_u$ of lost user data of an arbitrary entity is determined by

$$\breve{q}_u = \sum_{j=1}^{L} e_{s,j} \, \tilde{q}_{s,u} \left( \frac{e_{s,j}}{l \, s} \right) v_j \ . \tag{40}$$

It also holds that

$$E(\breve{Q}_{\text{DF}}) \approx \frac{C}{E(J)} \frac{P_{\text{DF}}}{\tilde{r}-d} \left( \prod_{j=1}^{\tilde{r}-1} V_j \right) \breve{q}_{\tilde{r}} \ , \tag{41}$$

where $C$ is determined by (2), $E(J)$ is determined by (15), $\tilde{q}_{s,u}(x)$ is determined by (34), and $P_u$, $P_{\text{DF}}$, and $V_j$ are determined by Equations (29), (23), and (60) of [6], respectively.

*Proof:* Equation (39) is obtained in Appendix. Equation (41) is obtained from (39) by setting $u = \tilde{r}$ and recognizing that $P_{\tilde{r}} = P_{\text{DF}}$. From (40), (12), it follows that $\breve{q}_{\tilde{r}} = E(e_s)$. ■

## V. NUMERICAL RESULTS

Here, we assess the reliability of the clustered and declustered placement schemes for the system and the parameter values considered in [6], as listed in Table II. The system is comprised of $n = 64$ devices (HDDs), it is protected by MDS erasure codes with $m = 16$ and $l = 13$, 14, 15 and employs a lazy rebuild scheme with a threshold $d = 0$, 1, and 2. Each HDD stores an amount of $c = 20$ TB with a sector (symbol) size $s$ of 512 bytes. The parameter $\lambda^{-1}$ is chosen to be equal to $876,000$ h (100 years) that corresponds to an AFR of 1%. Also, for an average reserved rebuild bandwidth $b$ of 100 MB/s, the mean rebuild time of a device is $\mu^{-1} = c/b = 55.5$ h, such that $\lambda/\mu = 6.3 \times 10^{-5} \ll 1$, which is a condition that ensures the accuracy of the reliability results obtained. Also, the rebuild time distribution is deterministic and sector errors are correlated with $f_{\text{cor}} \approx 1$.

First, we assess the reliability for the declustered placement scheme ($k = n = 64$) for the MDS-coded configurations considered in [6] with $m = 16$ and varying values of $l$ and $d$. These configurations are denoted by MDS($m$,$l$,$d$) and the corresponding results are shown in Figures 7 and 8 by solid lines for $d = 0$ (no lazy rebuild employed), dashed lines for $d = 1$ and dotted lines for $d = 2$. Six configurations are considered: MDS(16,13,0), MDS(16,13,1), MDS(16,13,2), MDS(16,14,0), MDS(16,14,1), and MDS(16,15,0), for each of the declustered and clustered data placement schemes. In particular, for the clustered placement scheme, the MDS(16,15,0) and MDS(16,14,0) configurations correspond to the RAID-5 and RAID-6 systems. The normalized EAFEL/$\lambda$ reliability metric corresponding to the declustered data placement scheme is obtained from (26) and shown in Figure 7(a) for a fixed entity size of $e_s = 10$ GB. In the interval $[10^{-15}, 10^{-12}]$ of practical importance for $P_{\text{b}}$, which is indicated between the two vertical dashed lines, EAFEL is degraded by orders of magnitude. Note that in the case of fixed-size entities, the EAFEL and EAFEDL metrics are the same, because the fraction of lost entities reflects the fraction of lost user data.

Next, we consider the case of a discrete bimodal distribution for the entity size, with $e_{s,1} = 1$ MB, $e_{s,2} = 1$ TB, and probabilities $v_1 \approxeq 0.99$ and $v_2 \approxeq 0.01$ chosen such that the average entity size $E(e_s)$ is $v_1 \, e_{s,1} + v_2 \, e_{s,2} = 10$ GB, the same as the entity size $e_s$ in the fixed-entity-size case considered previously. From (15), it follows that the average shard size $E(J)$ remains the same, which, according to (27), implies that the number $N_E$ of entities in the system remains the same as in the fixed-entity-size case. The resulting EAFEL is shown in Figure 7(b). Comparing the case of bimodal entity sizes with that of fixed entity sizes, we observe that, for $P_{\text{b}} < 10^{-14}$, reliability remains essentially the same, whereas for higher values of $P_{\text{b}}$, EAFEL is reduced. The reason for that is the following. For very small values of $P_{\text{b}}$, there can be at most one codeword lost, which results in one lost entity. Thus, the fraction of lost entities is $1/N_E$ in both cases. However, the lost entity in the fixed case has a size of 10 GB which is different from that of the lost entity in the bimodal case, which is either 1 MB or 1 TB. In fact, the size of the lost entity in the bimodal case is almost surely 1 TB, because the probability of this event is $v_2 \, e_{s,2}/E(e_s) \approx 1$. Consequently, the size of 1 TB of the lost entity in the bimodal case is 100 times larger than that of 10 GB of the entity lost in the fixed case. This is reflected in Figure 7(c) that shows the EAFEDL metric. Note that for $P_{\text{b}} = 10^{-15}$, indicated by the left vertical dashed line, EAFEDL is about 100 times larger than EAFEL. Consequently, in the case of variable size entities, it is more appropriate to consider the EAFEDL rather than the EAFEL metric, because it captures the amount of lost user data.

Clearly, the vulnerability of entities to loss increases with their size, which implies that lost entities are most likely large rather than small. For the case of the bimodal entity sizes, and for $v_2 \approxeq 0.01$, the number of the large 1-TB entities is significantly smaller than that of the 1-MB entities. We therefore deduce that the fraction of lost entities in the bimodal case is smaller than that for the fixed case, and this is more pronounced for larger values of $P_{\text{b}}$, as it is reflected by the EAFEL metric. By contrast, EAFEDL is larger in the bimodal case compared to the fixed case for the entire range of bit error rates. We therefore deduce that increasing the variability of the entity sizes, while keeping their average constant, results in degraded EAFEDL, but improved EAFEL, which is misleading. Clearly, the EAFEL metric that assesses the fraction of lost entities does not account for their size and the corresponding amount of lost user data and this led us to introduce the EAFEDL metric.

By observing Figures 8(a), 8(b) 8(c) that show the reliabil-

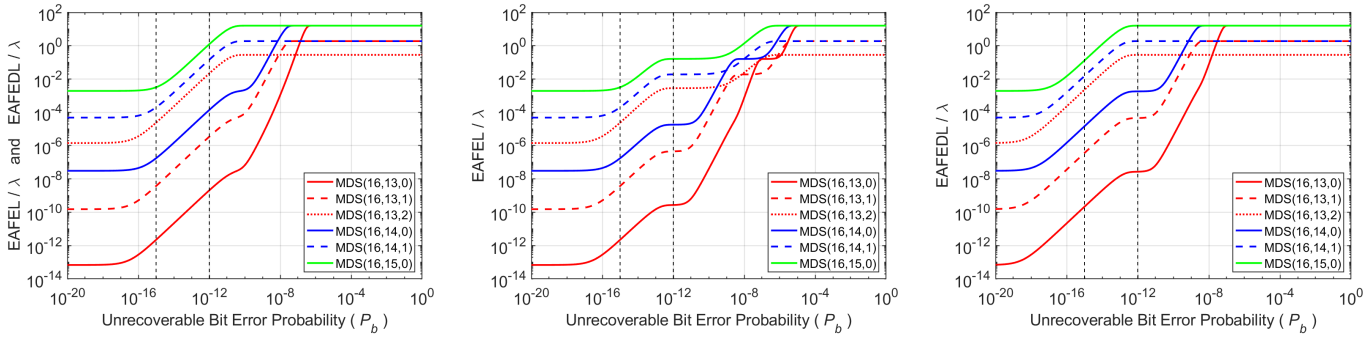


(a) Fixed Entity Size: $e_s = 10$ GB (b) Bimodal Entity Sizes: $e_{s,1} = 1$ MB, $e_{s,2} = 1$ TB (c) Bimodal Entity Sizes: $e_{s,1} = 1$ MB, $e_{s,2} = 1$ TB

Figure 7. Normalized EAFEL and EAFEDL vs. $P_{\text{b}}$ for various MDS$(m, l, d)$ codes; symbol size $s = 512$ B, declustered data placement.

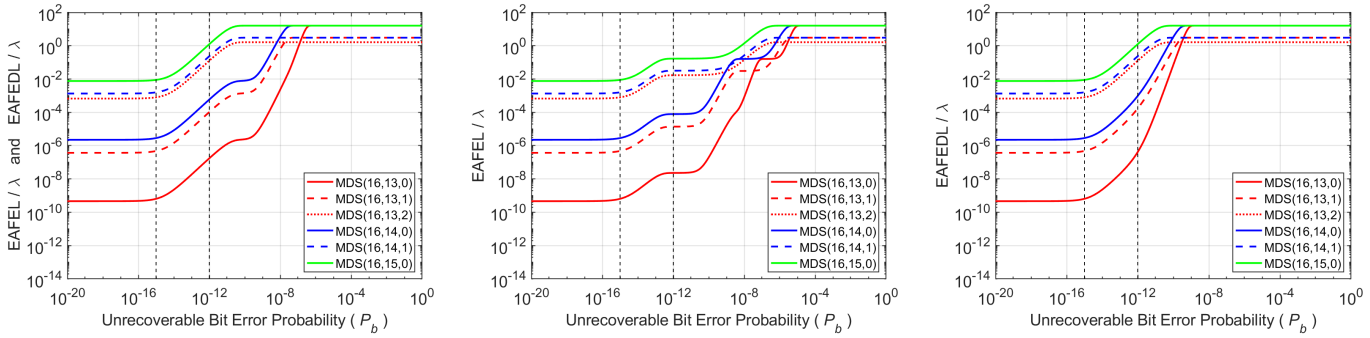


(a) Fixed Entity Size: $e_s = 10$ GB (b) Bimodal Entity Sizes: $e_{s,1} = 1$ MB, $e_{s,2} = 1$ TB (c) Bimodal Entity Sizes: $e_{s,1} = 1$ MB, $e_{s,2} = 1$ TB

Figure 8. Normalized EAFEL and EAFEDL vs. $P_{\text{b}}$ for various MDS$(m, l, d)$ codes; symbol size $s = 512$ B, clustered data placement.

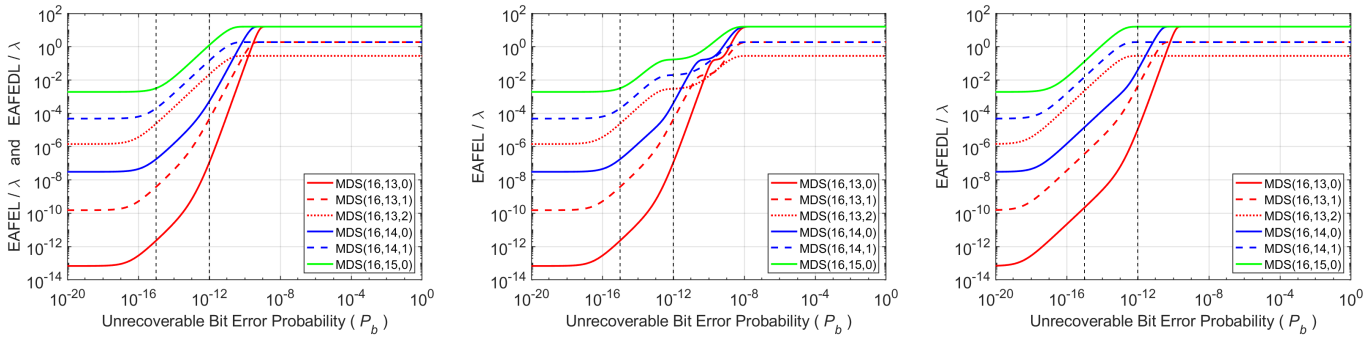


(a) Fixed Entity Size: $e_s = 10$ GB (b) Bimodal Entity Sizes: $e_{s,1} = 1$ MB, $e_{s,2} = 1$ TB (c) Bimodal Entity Sizes: $e_{s,1} = 1$ MB, $e_{s,2} = 1$ TB

Figure 9. Normalized EAFEL and EAFEDL vs. $P_{\text{b}}$ for various MDS$(m, l, d)$ codes; symbol size $s = 5$ MB, declustered data placement.

ity results for the case of clustered placement, we arrive to the same conclusions. From the above discussion, it follows that in the case of variable size entities, it is important to consider the EAFEDL rather than the EAFEL metric.

The effect of symbol size on reliability is assessed by considering the case of a large 5-MB symbol size. The corresponding normalized EAFEL$/\lambda$ and EAFEDL$/\lambda$ reliability metrics are shown in Figures 9 and 10. As expected, comparing these results with those shown in Figures 7 and 8, system reliability degrades compared to the case of a smaller symbol size. This degradation applies to both the EAFEL and EAFEDL reliability metrics.

Next, we assess the system reliability for the CERN file size distribution [9] that was considered in [10] and listed in Table III. For the file sizes uniformly distributed within the bins, the mean is equal to 843 MB, the standard deviation to 2.8 GB and the second moment to 8.9 GB$^2$. It turns out that the reliability metrics are extremely well approximated by considering the file sizes $e_{s,j}$ to be the bin mean sizes, such that $L = 38$. In this case, the mean is equal to 843 MB, the standard deviation to 2.8 GB and the second moment to 8.5 GB$^2$. The corresponding reliability results are shown in Figures 11 and 12. In all cases considered, the reliability level achieved by the declustered data placement scheme is higher than that of the clustered one.

## VI. Conclusions

The Expected Annual Fraction of Entity Loss EAFEL metric assesses the durability of data storage systems at an entity, say file, object, or block level. Contrary to the Mean Time to Data Loss (MTTDL) metric, EAFEL is affected by the distribution of the number of codewords that entities span. The distribution of this number was obtained analytically in closed

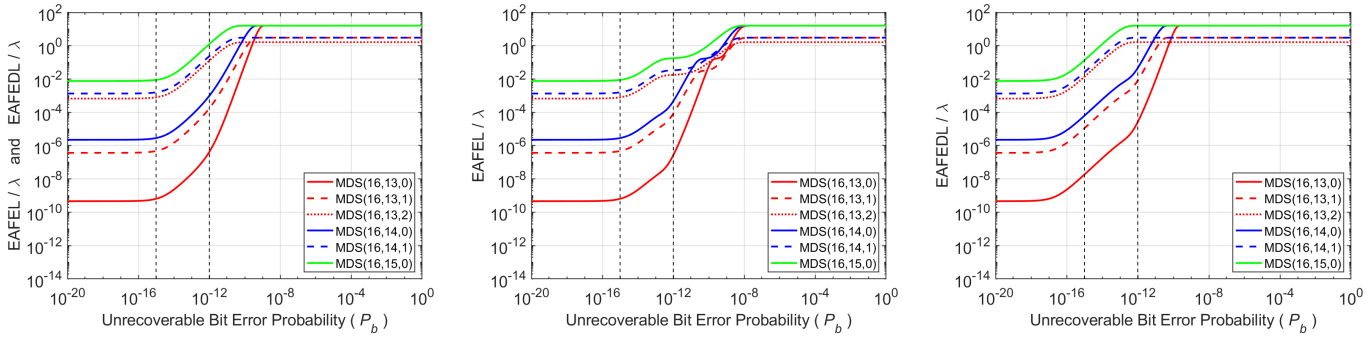


(a) Fixed Entity Size: $e_s = 10$ GB (b) Bimodal Entity Sizes: $e_{s,1} = 1$ MB, $e_{s,2} = 1$ TB (c) Bimodal Entity Sizes: $e_{s,1} = 1$ MB, $e_{s,2} = 1$ TB

Figure 10. Normalized EAFEL and EAFEDL vs. $P_{\rm b}$ for various MDS$(m, l, d)$ codes; symbol size $s = 5$ MB, clustered data placement.

form for the segregated and the random entity placement cases as a function of the size of the entities and the frequency of their occurrence. It was also demonstrated that, in certain cases of deterministic entity placements of variable-size entities, this distribution also depends on their actual placement.

To evaluate the durability of storage systems in the case of variable-size entities, a new reliability metric was introduced, the Expected Annual Fraction of Effective Data Loss (EAFEDL), which assesses the fraction of lost user data annually at the entity level. The EAFEL and the EAFEDL metrics were obtained analytically for erasure-coding redundancy schemes and for the clustered, declustered, and symmetric data placement schemes. Closed-form expressions capturing the effect of unrecoverable latent errors and lazy rebuilds were derived. We established that the reliability of storage systems is adversely affected by the presence of latent errors and that the declustered data placement scheme offers superior reliability. It was demonstrated that an increased variability of entity sizes results in improved EAFEL, but degraded EAFEDL. We established that EAFEL and EAFEDL are adversely affected by the symbol size. The analytical reliability results obtained enable the identification of erasure-coded redundancy schemes that ensure a desired level of reliability.

This work has the potential to be applied for further studies of data storage reliability and it is particularly relevant for tape storage reliability, which is a subject of further investigation.

TABLE III. CERN FILE SIZE DISTRIBUTION

| $j$ | Bins | | | Bin Mean Size $e_{s,j}$ | pdf $v_j$ |
|---|---|---|---|---|---|
| 1 | 1 B | – | 2 B | 2 B | 0.00004559 |
| 2 | 2 B | – | 5 B | 4 B | 0.00001275 |
| 3 | 5 B | – | 10 B | 8 B | 0.00005533 |
| 4 | 10 B | – | 22 B | 16.0 B | 0.00060401 |
| 5 | 22 B | – | 46 B | 34.0 B | 0.00018569 |
| 6 | 46 B | – | 100 B | 73.0 B | 0.00121244 |
| 7 | 100 B | – | 215 B | 157.5 B | 0.00093013 |
| 8 | 215 B | – | 464 B | 339.5 B | 0.00174431 |
| 9 | 464 B | – | 1 KB | 732.0 B | 0.00675513 |
| 10 | 1 KB | – | 2.154 KB | 1.577 KB | 0.00530524 |
| 11 | 2.154 KB | – | 4.642 KB | 3.398 KB | 0.00496005 |
| 12 | 4.642 KB | – | 10 KB | 7.321 KB | 0.00800625 |
| 13 | 10 KB | – | 21.544 KB | 15.772 KB | 0.01174913 |
| 14 | 21.544 KB | – | 46.416 KB | 33.980 KB | 0.01738480 |
| 15 | 46.416 KB | – | 100 KB | 73.208 KB | 0.01359001 |
| 16 | 100 KB | – | 215.443 KB | 157.721 KB | 0.01471745 |
| 17 | 215.443 KB | – | 464.159 KB | 339.801 KB | 0.02018806 |
| 18 | 464.159 KB | – | 1 MB | 732.079 KB | 0.02566358 |
| 19 | 1 MB | – | 2.154 MB | 1.577 MB | 0.06221012 |
| 20 | 2.154 MB | – | 4.642 MB | 3.398 MB | 0.07519022 |
| 21 | 4.642 MB | – | 10 MB | 7.321 MB | 0.07654035 |
| 22 | 10 MB | – | 21.544 MB | 15.772 MB | 0.09501620 |
| 23 | 21.544 MB | – | 46.416 MB | 33.980 MB | 0.07847651 |
| 24 | 46.416 MB | – | 100 MB | 73.208 MB | 0.07416942 |
| 25 | 100 MB | – | 215.443 MB | 157.721 MB | 0.09371673 |
| 26 | 215.443 MB | – | 464.159 MB | 339.801 MB | 0.08093624 |
| 27 | 464.159 MB | – | 1 GB | 732.079 MB | 0.05399279 |
| 28 | 1 GB | – | 2.154 GB | 1.577 GB | 0.04992384 |
| 29 | 2.154 GB | – | 4.642 GB | 3.398 GB | 0.08871583 |
| 30 | 4.642 GB | – | 10 GB | 7.321 GB | 0.03182476 |
| 31 | 10 GB | – | 21.544 GB | 15.772 GB | 0.00452804 |
| 32 | 21.544 GB | – | 46.416 GB | 33.980 GB | 0.00146156 |
| 33 | 46.416 GB | – | 100 GB | 73.208 GB | 0.00017060 |
| 34 | 100 GB | – | 215.443 GB | 157.721 GB | 0.00001375 |
| 35 | 215.443 GB | – | 464.159 GB | 339.801 GB | 0.00000206 |
| 36 | 464.159 GB | – | 1 TB | 732.079 GB | 0.00000069 |
| 37 | 1 TB | – | 2.154 TB | 1.577 TB | 0.00000033 |
| 38 | 2.154 TB | – | 4.310 TB | 3.230 TB | 0.00000001 |

## APPENDIX

**Proof of Propositions 1 and 2.**

Upon entering exposure level $u$ $(u \geq d+1)$, there are $C_u$ most-exposed codewords to be recovered. As a shard size of $s_s$ corresponds to $J$ symbols, an entity size $e_s$ corresponds to $J$ codewords. Therefore, the average entity of size $E(e_s)$ determined by (12) corresponds to $E(J)$ codewords, with $E(J)$ determined by (15). Consequently, for the number $E_u$ of entities to be recovered it holds that

$$E_u \approx \frac{C_u}{E(J)}, \quad \text{for } u = d+1, \ldots, \tilde{r}-1 . \tag{42}$$

Let $K$ $(K \geq 1)$ denote the number of codewords that an entity of size $e_s$ spans or, equivalently, the number of symbols that a shard of size $s_s$ spans. The entity is lost if any of these $K$ codewords is permanently lost. Therefore, according to Equation (98) of [4], the probability of recovering the entity is $q_u^{f_{\rm cor}\,K}$, where $q_u$ is the probability of restoring a codeword and is determined by (35), and $f_{\rm cor}$ accounts for the correlation of latent errors and is determined by Equation (29) of [4]. Consequently, the probability $\tilde{q}_u|K$ of loss of an entity that spans $K$ codewords is determined by

$$\tilde{q}_u|K \;=\; 1 - q_u^{f_{\rm cor}\,K} . \tag{43}$$

Unconditioning (43) on $K$ using (22) yields the probability $\tilde{q}_{s,u}(J)$ that the entity (for the shard size $J$) is lost, where $\tilde{q}_{s,u}(x)$ is determined by (34). Thus, using (4), the probability $\tilde{q}_u(e_s)$ that the entity is lost is determined by

$$\tilde{q}_u(e_s) \;=\; \tilde{q}_{s,u}\left(\frac{e_s}{l\,s}\right) . \tag{44}$$

For this entity, the expected amount $\breve{q}_u(e_s)$ of lost user data is

$$\breve{q}_u(e_s) \;=\; e_s\,\tilde{q}_u(e_s) . \tag{45}$$

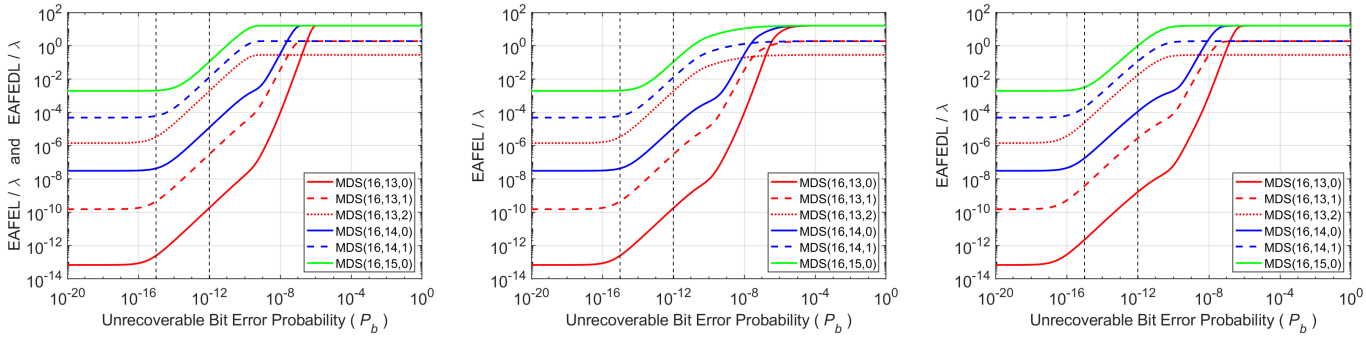


(a) Fixed File Size: $e_s = 843$ MB (b) CERN File Sizes; $E(e_s) = 843$ MB (c) CERN File Sizes; $E(e_s) = 843$ MB

Figure 11. Normalized EAFEL and EAFEDL vs. $P_{\rm b}$ for various MDS$(m, l, d)$ codes; symbol size $s = 512$ B, declustered data placement.

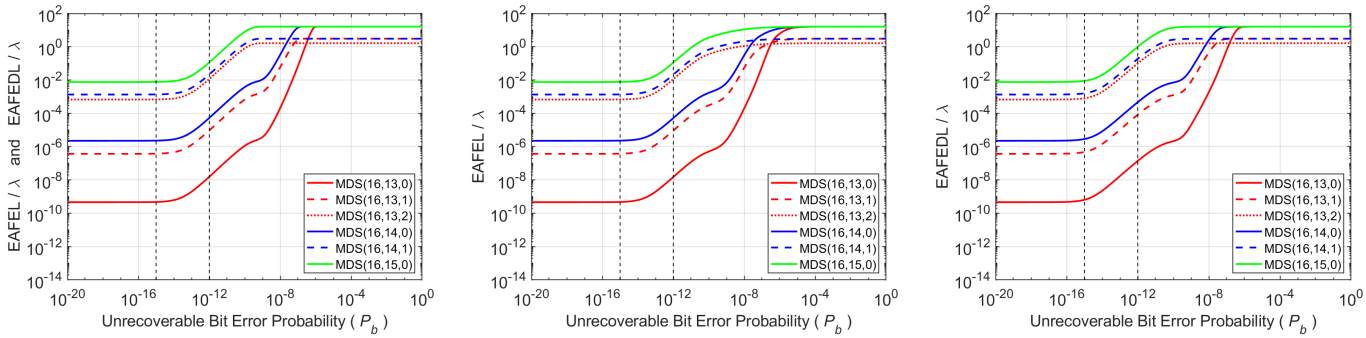


(a) Fixed File Size: $e_s = 843$ MB (b) CERN File Sizes; $E(e_s) = 843$ MB (c) CERN File Sizes; $E(e_s) = 843$ MB

Figure 12. Normalized EAFEL and EAFEDL vs. $P_{\rm b}$ for various MDS$(m, l, d)$ codes; symbol size $s = 512$ B, clustered data placement.

From (11), the probability $\tilde{q}_u$ that an arbitrary entity is lost is

$$\tilde{q}_u = \sum_{j=1}^{L} \tilde{q}_u(e_{s,j})\, v_j \ , \tag{46}$$

which, using (44), yields (33).

Similarly, from (11), it follows that the expected amount $\breve{q}_u$ of lost user data of an arbitrary entity is determined by

$$\breve{q}_u = \sum_{j=1}^{L} \breve{q}_u(e_{s,j})\, v_j \ , \tag{47}$$

which, using (44) and (45), yields (40).

Let $Y_{\rm U}$ be the number of lost entities and $\breve{Q}_{\rm U}$ the amount of lost user data at exposure level $u$ during the rebuild process of the $C_u$ codewords. Then it holds that,

$$E(Y_{\rm U}|C_u) \ = \ E_u\, \tilde{q}_u \ \overset{(42)}{\approx} \ \frac{C_u}{E(J)}\, \tilde{q}_u \ , \tag{48}$$

and

$$E(\breve{Q}_{\rm U}|C_u) \ = \ E_u\, \breve{q}_u \ \overset{(42)}{\approx} \ \frac{C_u}{E(J)}\, \breve{q}_u \ . \tag{49}$$

Note that $E(Y_{\rm U}|C_u)$, as determined by (48), can be obtained from Equation (71) of [6] by replacing the shard size $J$ with its average value $E(J)$. Consequently, (32) and (36) are obtained from the corresponding Equations (42) and (44) of [6] by replacing the shard size $J$ with its average value $E(J)$.

Note also that $E(\breve{Q}_{\rm U}|C_u)$, as determined by (49), can be obtained from (48) by replacing the probability $\tilde{q}_u$ that an arbitrary entity is lost with its expected amount $\breve{q}_u$ of lost user data. Consequently, (39) is obtained from (32) by replacing $\tilde{q}_u$ with $\breve{q}_u$.

## REFERENCES


[1] I. Iliadis and V. Venkatesan, "Reliability evaluation of erasure coded systems," Int'l J. Adv. Telecommun., vol. 10, no. 3&4, Dec. 2017, pp. 118–144.

[2] I. Iliadis, "Reliability evaluation of erasure coded systems under rebuild bandwidth constraints," Int'l J. Adv. Networks and Services, vol. 11, no. 3&4, Dec. 2018, pp. 113–142.

[3] ——, "Reliability of erasure-coded storage systems with latent errors," Int'l J. Adv. Telecommun., vol. 15, no. 3&4, Dec. 2022, pp. 23–41.

[4] ——, "Reliability evaluation of erasure-coded storage systems with latent errors," ACM Trans. Storage, vol. 19, no. 1, Jan. 2023, pp. 1–47.

[5] I. Iliadis and V. Venkatesan, "Expected annual fraction of data loss as a metric for data storage reliability," in Proc. 22nd Annual IEEE Int'l Symposium on Modeling, Analysis, and Simulation of Computer and Telecommunication Systems (MASCOTS), Sep. 2014, pp. 375–384.

[6] I. Iliadis, "Expected annual fraction of entity loss as a metric for data storage durability," in Proc. 16th Int'l Conference on Communication Theory, Reliability, and Quality of Service (CTRQ), Apr. 2023, pp. 1–11.

[7] G. A. Jaquette, "LTO: A better format for mid-range tape," IBM J. Res. Dev., vol. 47, no. 4, Jul. 2003, pp. 429–444.

[8] Tape Roadmap, Information Storage Industry Consortium (INSIC) Report, 2019. [Online]. Available: https://www.insic.org/wp-content/uploads/2019/07/INSIC-Applications-and-Systems-Roadmap.pdf [retrieved: March, 2024]

[9] G. Cancio et al., "Tape archive challenges when approaching exabyte-scale," 2010, Presentation at CHEP 2010, available online.

[10] I. Iliadis, L. Jordan, M. Lantz, and S. Sarafijanovic, "Performance evaluation of automated tape library systems," in Proc. 29th IEEE International Symposium on Modeling, Analysis, and Simulation of Computer and Telecommunication Systems (MASCOTS), Nov. 2021, pp. 1–8.